Potential Adsorbent for Light Hydrocarbon Separation: Role of SBA-15 Framework Porosity

Bharat L. Newalkar,[†,||] Nettem V. Choudary,[‡,||] Uday T. Turaga,[§] R. P. Vijayalakshmi,[‡] Prakash Kumar,[‡] S. Komarneni,*[,†] and Thirumaleshwara S. G. Bhat*[,‡]

Materials Research Laboratory, Materials Research Institute, The Pennsylvania State University, University Park, Pennsylvania 16802, Research Centre, Indian Petrochemicals Corporation Limited, Vadodara 391346, India, and Fuel Science Program, Department of Energy and Geo-Environmental Engineering, The Pennsylvania State University, University Park, Pennsylvania 16802

Received September 3, 2002. Revised Manuscript Received January 6, 2003

Samples of mesoporous silica SBA-15 with and without controlled framework microporosity were prepared under microwave hydrothermal conditions. These samples were evaluated for their ability to separate ethane and ethylene by obtaining their equilibrium adsorption isotherms using volumetric adsorption at 303 and 323 K, respectively. The data obtained were analyzed using the Langmuir−Freundlich adsorption isotherm model. Although the mesoporous silica samples showed a higher adsorption capacity for ethylene, it was found to decrease upon reduction in the adsorbent's framework microporosity. Likewise, the isosteric heats of adsorption estimated by the Clausius−Clapeyron equation are higher for ethylene as compared to those for ethane and were also found to depend on framework microporosity. The sample with higher microporosity displayed strong affinity for ethylene and is comparable with those reported for π-complexation-based systems. This affinity was observed to weaken on the sample with lower microporosity and absent altogether on the micropore-free SBA-15 sample. Furthermore, the affinity of the micropore-free SBA-15 framework for ethylene and ethane was observed to be similar to and comparable with those obtained on MCM-41 type mesoporous silica. The thus-obtained trend has revealed the importance of framework microporosity in designing a SBA-15-based adsorbent for ethane/ethylene separation.

Introduction

The discovery of ordered, hydrothermally stable mesoporous silica, SBA-15, has generated tremendous interest in the field of catalysis, separation science, and advanced materials.[1] Owing to this, attempts have been made to prepare Al-, V-, and Ti-substituted SBA-15 frameworks to exploit their catalytic potential.[2−7] Likewise, surface modification of SBA-15 framework has been performed via bonding of organosilanes[7−13] for heavy metal remediation, sequestration, and controlled release of proteins. Such materials have also exhibited facile catalytic properties. Furthermore, SBA-15 has also been found applicable as a waveguide and mirrorless laser.[14] It has been successfully employed as a host to prepare mesoporous carbon, metal nanowires, and nanoballs.[15−18] Such a wide range of applications has motivated research on new synthetic methods for the

* Authors for correspondence. S. Komarneni: Phone 1-814-865-1542; fax 1-814-865-2326; E-mail komarneni@psu.edu. T. S. G. Bhat: Phone 011-91-265-262011 ext. 3673; fax 011-91-265-262098; e-mail sgtbhat@ipclmail.com.

† Materials Research Institute, The Pennsylvania State University.

‡ Indian Petrochemicals Corporation Limited.

§ Department of Energy and Geo-Environmental Engineering, The Pennsylvania State University.

|| Present address: Corporate R&D, Bharat Petroleum Corporation Limited, Plot 2A, Udyog Kendra, Greater Noida, India.

(1) (a) Zhao, D.; Feng, J.; Huo, Q.; Melosh, N.; Fredrickson, G. H.; Chmelka, B. F.; Stucky, G. D. *Science* **1998**, *279*, 548. (b) Zhao, D.; Huo, Q.; Feng, J.; Chmelka, B. F.; Stucky, G. D. *J. Am. Chem. Soc.* **1998**, *120*, 6024.

(2) Luan, Z.; Maes, E. M.; van der Heide, P. A. W.; Zhao, D.; Czernuszewicz, R. S.; Keven, L. *Chem. Mater.* **1999**, *11*, 3680.

(3) Cheng, M.; Wang, Z.; Sakurai, K.; Kumata, F.; Saito, T.; Komatsu, T.; Yashima, T. *Chem. Lett.* **1999**, 131.

(4) Yue, Y.; Gedeon, A.; Bonardet, J.-L.; Melosh, N.; D'Espinose, J.-B.; Fraissard, J. *Chem. Commun.* **1999**, 1967.

(5) (a) Luan, Z.; Hartmann, M.; Zhao, D.; Zhou, W.; Kevan, L. *Chem. Mater.* **1999**, *11*, 1621. (b) Newalkar, B. L.; Olanrewaju, J.; Komarneni, S. *Chem. Mater.* **2001**, *13*, 552.

(6) Morey, M. S.; O'Brien, S.; Schwarz, S.; Stucky, G. D. *Chem. Mater.* **2000**, *12*, 898.

(7) Luan, Z.; Bae, J. Y.; Kevan, L. *Chem. Mater.* **2000**, *12*, 3202.

(8) (a) Bae, S. J.; Kim, S.-W.; Hyeon, T.; Kim, B. M. *Chem. Commun.* **1999**, *31*. (b) Park, M.; Komarneni, S. *Microporous Mesoporous Mater.* **1998**, *25*, 75.

(9) Liu, A. M.; Hidajat, K.; Kawi, S.; Zhao, D. Y. *Chem. Commun.* **2000**, 1145.

(10) Han, Y.-J.; Stucky, G. D.; Butler, A. *J. Am. Chem. Soc.* **1999**, *121*, 9897.

(11) Lin, H.-P.; Yang, L.-Y.; Mou, C.-Y.; Liu, S.-B.; Lee, H.-K. *New J. Chem.* **2000**, *24*, 253.

(12) Margolese, D.; Melero, J. A.; Christiansen, S. C.; Chmelka, B. F.; Stucky, G. D. *Chem. Mater.* **2000**, *12*, 2448.

(13) Markowitz, M. A.; Klaehn, J.; Hendet, R. A.; Qadriq, S. B.; Golledge, S. L.; Castner, D. G.; Gaber, B. P. *J. Phys. Chem. B* **2000**, *104*, 10820.

(14) Yang, P.; Wirrnsberger, G.; Huang, H. C.; Cordero, S. R.; McGehee, M. D.; Scott, B.; Deng, T.; Whitesides, G. M.; Chemelka, B. F.; Buratto, S. K.; Stucky, G. D. *Science* **2000**, *287*, *465*.

(15) Shinae Jun, S.; Joo, S. H.; Ryoo, R.; Kruk, M.; Jaroniec, M.; Liu, Z.; Ohsuna, T.; Terasaki, O. *J. Am. Chem. Soc.* **2000**, *122*, 10712.

(16) Han, Y.-J.; Kim, J. M.; Stucky, G. D. *Chem. Mater.* **2000**, *12*, 2068.

(17) Kang, H.; Jun, Y.-W.; Park, J.; Lee, K.-B.; Cheon, J. *Chem. Mater.* **2000**, *12*, 3530.

10.1021/cm020889d CCC: $25.00
Published on Web 03/07/2003

development of these materials in various meso- and macroscopic forms.[19]

In comparison to these ongoing efforts, attempts to understand the adsorption potential of SBA-15 are sparse. Recently, we investigated the adsorption properties of SBA-15 to evaluate its potential for the separation of commercially important light hydrocarbons such as C_2 and C_3.[20] Interestingly, this study revealed a high affinity of SBA-15 framework for light alkenes over corresponding alkanes and was in line with those observed on π-complexation-based systems. The cause for such high affinity of the SBA-15 framework for light alkenes was judged in terms of its textural characteristics but was not proven. Therefore, the main objective of the present study is to investigate the role of textural characteristics, especially framework microporosity, of SBA-15, in determining the adsorption potential for light hydrocarbons. Thus, equilibrium adsorption isotherms for ethane and ethylene were measured using volumetric adsorption at 303 and 323 K, respectively, on SBA-15 samples having varying degrees of framework microporosity. The resultant data were analyzed using the Langmuir−Freundlich adsorption isotherm model. Furthermore, equilibrium adsorption isotherms were measured on MCM-41-type mesoporous silica to understand the role of framework microporosity. The isosteric heats of adsorption and adsorption capacity were estimated to understand the role of framework microporosity in determining the SBA-15 framework's adsorption affinity for light alkenes.

Experimental Section

Sample Preparation. Siliceous SBA-15 sample was prepared by templating tetraethyl orthosilicate (TEOS, Aldrich), with a triblock poly(ethyleneoxide)−poly(propyleneoxide)−poly(ethyleneoxide) ($EO_{20}PO_{70}EO_{20}$, MW 5800, Aldrich) under microwave-hydrothermal conditions by following the synthetic procedure described elsewhere.[21] Microwave-hydrothermal synthesis was performed using a MARS5 (CEM Corp., Matthews, NC) microwave digestion system. The SBA-15 sample thus obtained is hereafter referred to as S0.

SBA-15 samples with controlled framework microporosity were prepared by adopting a recently developed in situ synthesis approach under microwave-hydrothermal conditions.[22] Briefly, a gel having composition of $EO_{20}PO_{70}EO_{20}$ polymer/SiO_2/NaCl/HCl/ethanol/H_2O (1 g (0.17 mmol):0.010 mol:*x* mmol:0.06 mol:44 mmol:1.88 mol ($x = 7.7$ and 15.5) was prepared using tetraethyl orthosilicate as the silica source. The resultant gel was then stirred overnight at ambient conditions and subjected to microwave-hydrothermal conditions. Microwave-hydrothermal synthesis was performed using the MARS5 microwave digestion system, wherein an in-situ monitoring of the temperature and pressure was performed through a pressure sensor and a fiber optic temperature probe. The microwave-hydrothermal synthesis was performed under static conditions at 373 K for 2 h using 300 W of microwave power. The samples obtained with 7.7 and 15.5 mmol of sodium chloride were designated S1 and S2, respectively.

Siliceous MCM-41 sample was prepared by employing cetyltrimethylammonium bromide (CTAB, Aldrich) as a structure-directing agent and fumed silica (Cab-O-Sil) as the silica source. Typically, a gel with a composition[23] of SiO_2/TMAOH/CTAB/H_2O (1.00:0.19:0.27:40) was subjected to crystallization under microwave-hydrothermal conditions at 438 K for 4 h.

All the crystallized products were filtered, washed with warm distilled water, dried at 383 K, and finally calcined at 813 K in air for 6 h. The calcined materials were then used for characterization studies.

Characterization. X-ray diffraction patterns for the SBA-15 and MCM-41 samples were recorded using a Philips X'pert powder diffractometer system with Cu Kα radiation with a 0.02° step size and 1 s step time over the range $0.5° < 2\theta < 6°$. The sodium content of various adsorbent samples was determined using atomic absorption spectroscopy. The textural properties of the samples were evaluated using nitrogen adsorption/desorption measurements with an Autosorb-1 (Quantachrome) unit. Nitrogen adsorption/desorption isotherms were measured at 77 K after degassing samples below 10^{-3} Torr at 473 K for 4 h. The BET specific surface area (S_{BET}) was estimated using adsorption data in a relative pressure range from 0.04 to 0.2. The external surface area, S_{ex}, total surface area, S_t, primary mesopore surface area, S_p, micropore volume, V_{mi}, and primary mesopore volume, V_p, were estimated using the α_s-plot method, as described elsewhere.[24,25] Amorphous nonporous silica (Thiokol, $S_{BET} = 7.0$ m^2/g) was used as a reference adsorbent. The mesopore size distribution (PSD) was obtained by analyzing the adsorption data of the N_2 isotherm using the recently developed KJS (Kruk, Jaroniec, and Sayari) approach.[26] The pore diameter corresponding to the maximum of PSD is denoted as W_{KJS}. The total pore volume, V_t, was estimated from the amount adsorbed at a relative pressure of 0.95.

Adsorption Isotherms Measurements. Adsorption isotherms for ethane and ethylene were measured using a volumetric adsorption measurement unit at 303 and 323 K, respectively. Typically, about 1 g of activated sample was loaded in a volumetric adsorption unit, which was fitted with two absolute pressure transducers (MKS model 122AA) in the 100 and 1000 mmHg range with an accuracy of 0.01 and 0.1 mmHg, respectively). The sample temperature was maintained within 0.01 K using a JULABO F10 thermostatic circulating bath. All the adsorbates used in the present study were UHP grade (purity > 99.99%). At the end of the adsorption run, desorption was carried out to check the reversibility of the adsorption isotherm. All the measurements were performed in duplicate to ensure the quality and reproducibility of the data. The measured adsorption data were analyzed using the Langmuir−Freundlich adsorption isotherm model.

Results and Discussion

Adsorbent Characterization. Calcined SBA-15 and MCM-41 samples displayed well-resolved patterns comprising of a sharp and two long order weak peaks in agreement with previously reported patterns. The XRD peaks are indexed to a hexagonal lattice with d(100) spacing corresponding to a large unit cell parameter,

(18) Jang, J. S.; Lim, B.; Lee, J.; Hyeon, T. *Chem. Commun.* **2001**, 83.

(19) (a) Lu, Y.; Gangulli, R.; Drewien, C. A.; Anderson, M. T.; Brinker, C. J.; Gong, W.; Guo, Y.; Soyez, H.; Dunn, B.; Huang, M. H.; Zink, J. I. *Nature* **1997**, *389*, 364. (b) Ogawa, M.; Igarashi, T.; Kuroda, K. *Bull. Chem. Soc. Jpn.* **1997**, *70*, 2833. (c) Zhao, D.; Yang, P.; Melosh, N.; Feng, J.; Chmelka, B. F.; Stucky, G. D. *Adv. Mater.* **1998**, *10*, 1380. (d) Tolbert, S. H.; Firouzi; Stucky, G. D.; Chmelka, B. F. *Science* **1997**, *278*, 264. (e) Attard, G. S.; Glyde, J. C.; Göltner, C. G. *Nature* **1995**, *378*, 366. (f) Feng, P.; Bu, X.; Stucky, G. D.; Pine, D. J. *J. Am. Chem. Soc.* **2000**, *122*, 994.

(20) Newalkar, B. L.; Choudary, N. V.; Kumar, P.; Komarneni, S.; Bhat, S. G. T. *Chem. Mater.* **2002**, *14*, 304.

(21) Newalkar, B. L.; Komarneni, S.; Katsuki, H. *Chem. Commun.* **2000**, 2389.

(22) Newalkar, B. L.; Komarneni, S. *Chem. Mater.* **2001**, *13*, 4573.

(23) Pauly, T. R.; Petkov, V.; Liu, Y.; Billinge, S. J. L.; Pinnavaia, T. J. *J. Am. Chem. Soc.* **2002**, *124*, 97.

(24) Gregg, S. J.; Sing, K. S. W. *Adsorption, Surface Area and Porosity*; Academic Press: New York, 1982.

(25) Sayari, A.; Liu, P.; Kruk, M.; Jaroniec, M. *Langmuir* **1997**, *13*, 2499.

(26) Kruk, M.; Jaroniec, M.; Sayari, A. *Langmuir* **1997**, *13*, 6267.

Table 1. Textural Parameters for Various Adsorbent Samples[a]

sample	a_o (Å)	W_{KJS} (Å)	V_t at $p/P = 0.95$ (cm^3/g)	V_p (cm^3/g)	V_{mi} (cm^3/g)	S_{BET} (m^2/g)	S_t (m^2/g)	S_{ex} (m^2/g)	S_p (m^2/g)	$(W_{KJS}S_p)/V_p$
S0	105.0	73	0.97	0.88	0.04	791	812	24.4	788	6.53
S1	84.2	52	0.51	0.44	0.02	517	527	37	490	5.7
S2	84.2	52	0.43	0.39	~0	336	341	19	322	4.2
MCM-41	59.0	40	0.76	0.76	0	734	795	16	779	4.1

[a] $a_o = 2d_{100/\sqrt{3}}$. $S_p = S_t - S_{ex}$.

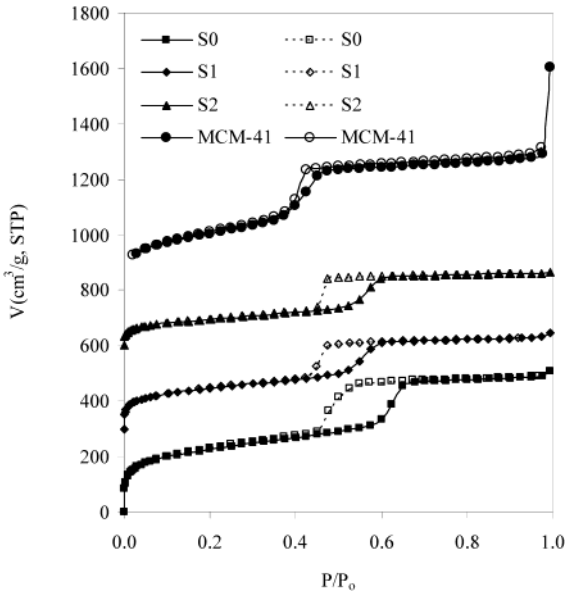

Figure 1. Nitrogen adsorption/desorption isotherm for various adsorbent samples obtained under microwave-hydrothermal conditions at 77 K. The adsorption/desorption isotherms for samples S0, S1, S2, and MCM-41 are shifted by 0, 300, 600, and 800 cm^3 STP/g, respectively (closed symbol represents adsorption branch; open symbol represents desorption branch).

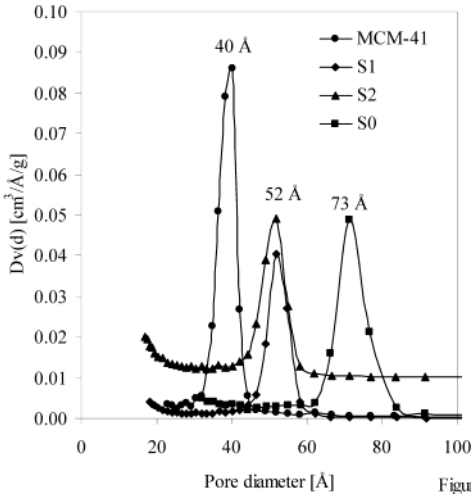

Figure 2. Pore-size distribution for various adsorbent samples based on KJS approach. The PSD curve for adsorbent S2 is shifted by 0.01 cm^3/Å/g.

a_o (Table 1). The sodium contents in the S0, S1, and S2 samples were found to be 0, 0.2, and 0.4 wt %, respectively. All the synthesized samples exhibited uniform pore size distribution (Figure 2) and a typical Type IV adsorption−desorption isotherm of nitrogen characteristic of a mesoporous solid (Figure 1). Furthermore, nitrogen adsorption isotherms for SBA-15 displayed a H1 hysteresis loop, which is typical of mesoporous solids.[24] The estimated textural parameters such as specific surface area, S_{BET}, total surface area, S_t, external surface area, S_{ex}, primary mesopore volume, V_p, micropore volume, V_{mi}, total pore volume, V_p, and mesopore size, W_{KJS}, are compiled in Table 1. Interestingly, the estimated micropore volumes for S0 and S1 samples were found to be significantly lower than those observed for samples obtained under conventional hydrothermal conditions. As reported earlier, the unit cell parameters and textural properties for the samples S1 and S2 are found to be lower than those observed for S0. Furthermore, the ratio of $W_{KJS}S_p/V_p$ is about 5.5, 4.2, and about 4.0 for the S1, S2, and MCM samples, respectively. This in turn reflected the crystallization of a uniform hexagonally packed cylindrical pore network for sample S2, which could have a close structural resemblance with MCM-41. (Note that for an array of hexagonally packed cylindrical pores of MCM-41-type material, the $W_{KJS}S_p/V_p$ ratio is about 4.0, whereas it is higher for SBA-15 due to the presence of framework porosity). These results are in good agreement with those reported earlier[22] and also confirmed the structural as well as the adsorption crystallinity of the adsorbent. The presence of micropore-free framework in sample S2 is further confirmed by the platinum inverse replication method[27] wherein the formation of individual Pt-nanowires (Figure 3) having a diameter of about 5.5 nm is observed.

Adsorption Isotherms of C_2 Hydrocarbons. Figure 4 depicts the adsorption isotherms for C_2 adsorbates measured at 303 and 323 K on various adsorbents. The equilibrium adsorption capacities for these adsorbates on various adsorbents at 1 atm are compiled in Table 2. The isotherms show that the adsorption capacity for ethylene is substantially higher than that for ethane on the S0 sample. However, such capacity is found to decrease progressively on the S1 and S2 samples. Interestingly, the adsorption capacity for ethylene on MCM-41 is found to be higher as compared to that noticed for MCM-41 like SBA-15 sample (S2). This reflects the important role of surface area (Table 1) for alkene uptake. To judge the role of sodium ions on olefin uptake, the measured data are compared with the one reported on Na^+-zeolite Y.[29] The reported equilibrium capacities at 1 atm for ethane and ethylene on Na^+-zeolite Y were observed to be 2.3 and 1.8 mmol/g,

(27) (a) Liu, Z.; Terasaki, O.; Ohsuna, T.; Hiraga, K.; Shin, H. J.; Ryoo, R. *Chem. Phys. Chem.* **2001**, *4*, 229. (b) Liu, Z.; Sakamoto, Y.; Ohsuna, T.; Hiraga, K.; Terasaki, O.; Ko, C. H.; Shin, H. J.; Ryoo, R. *Angew. Chem. Int. Ed.* **2000**, *39*, 3107. (c) Ryoo, R.; Jun, S. *J. Phys. Chem. B* **1997**, *101*, 317.

(28) (a) Impéror-Clerc, M.; Davidson, P.; Davidson, A. *J. Am. Chem. Soc.* **2000**, *122*, 11925. (b) Kruk, M.; Jaroniec, M.; Ko, C. H.; Ryoo, R. *Chem. Mater.* **2000**, *12*, 1961.

(29) Yang, R. T.; Kikkinides, E. S. *AIChE J.* **1995**, *41*, 509.

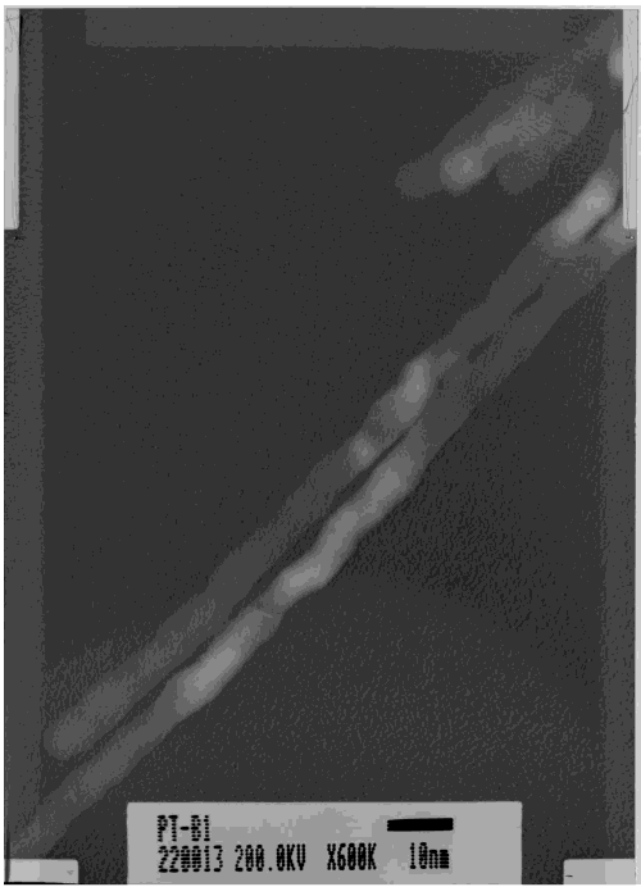

Figure 3. Transmission electron micrograph for Pt-nanowires produced from micropore free SBA-15 (Sample S2) framework.

respectively, which are higher than those observed for S0 and MCM-41 (Table 2). However, a poor selectivity ratio of ethylene/ethane has been reported on Na^+-zeolite Y system. Furthermore, the selectivity for olefin is reported to be increased via π-complexation through Cu^+/Ag^+ ion exchange. Therefore, the presence of sodium in S1 and S2 samples is not believed to have any significant role during ethane and ethylene uptake.

Evaluation of Equilibrium Isotherm Model. The adsorption data were analyzed using the Langmuir and Langmuir−Freundlich models by the nonlinear regression approach. The experimental data were well represented by the Langmuir−Freundlich adsorption isotherm model, i.e., $V=V_m\, bp^n/(1 + bp^n)$, where V is the amount adsorbed at equilibrium pressure p in mmHg, V_m is the monolayer adsorption capacity in mmol/g, and b and n are Langmuir and Freundlich constants, respectively. The equilibrium adsorption parameters so obtained are also compiled in Table 2. It can be seen that the Langmuir−Freundlich constant, b, which is a measure of interaction between adsorbate and adsorbent for ethylene is found to increase gradually in the order of S2 < S1 < S0 for various samples. This in turn suggested a stronger interaction of ethylene molecules with the adsorbent surface as a function of framework porosity. In other words, the interaction of alkenes with the surface of the adsorbent having higher framework porosity is stronger than that with an adsorbent having lower framework porosity. This trend strongly suggests the important role of framework porosity in determining olefin uptake on SBA-15-type frameworks.

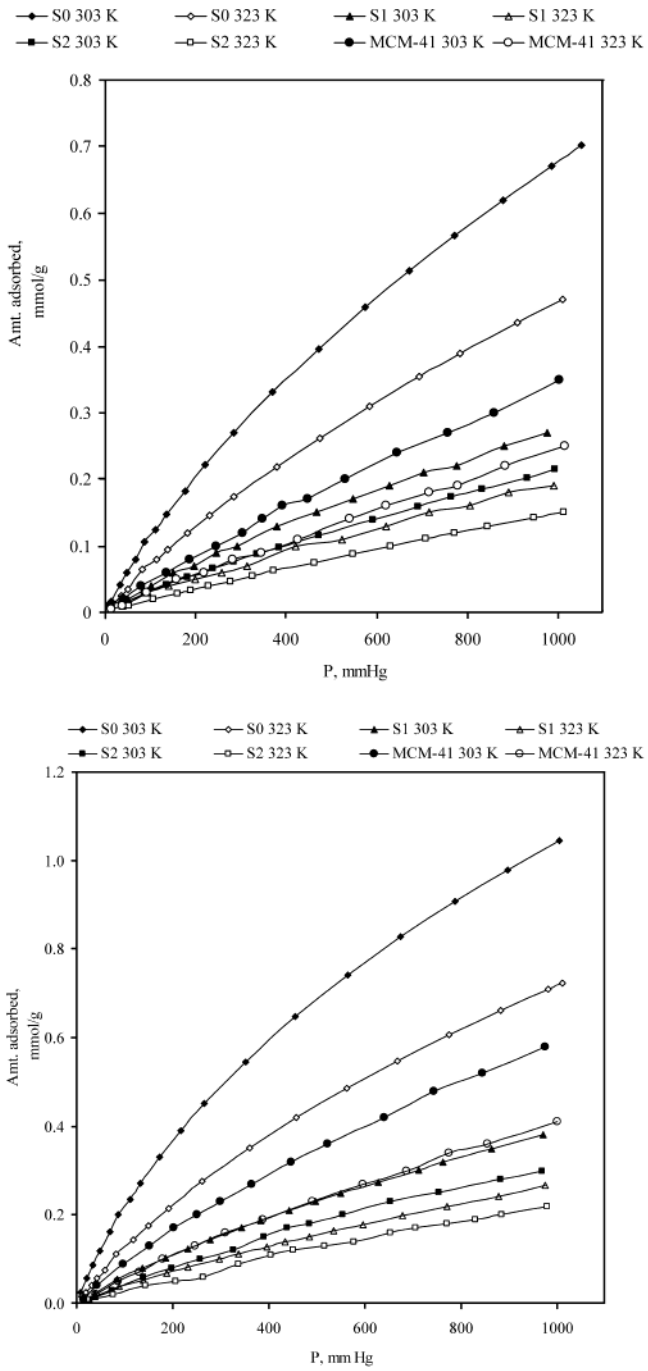

Figure 4. Equilibrium adsorption isotherms for (a) ethane and (b) ethylene on various adsorbents at 303 and 323 K.

Isosteric Heats of Adsorption. The isosteric heats of adsorption (ΔH) for various adsorbates are estimated using the Clausius−Clapeyron equation (Table 2) and their dependence on adsorption coverage is shown in Figure 5. The heats of adsorption for ethylene on S0, S1, S2, and MCM-41 samples were 8.4, 6.2, 4.6, and 5.0 kcal/mol, respectively, whereas those for ethane were 5.9, 5.8, 4.7, and 4.2 kcal/mol, respectively. The isosteric heats of adsorption are found to be higher for ethylene compared to ethane over the entire adsorption coverage. Furthermore, a sharp drop in the heats of adsorption for ethylene is noticed on S0 with an increase in adsorption coverage, which reflected the presence of surface heterogeneity in the form of specific adsorption sites. Interestingly, such a sharp drop was not signifi-

Table 2. Isosteric Heats (ΔH) of Adsorption at Low Coverage, Equilibrium Adsorption Capacities (Q) at 1 Atm, and Fitted Langmuir−Freundlich Constants (V_m, b, and n) for C2 Hydrocarbons on Various Mesoporous Silica Adsorbents

adsorbent	adsorbate	ΔH (kcal/mol)	T (K)	Q (mmol/g)	V_m (mmol/g)	$b \times 10^3$ ($mmHg^{1-}$)	n
S0	ethane (C_2H_6)	5.9	303	0.56	2.72	0.75	0.88
			323	0.38	2.62	0.45	0.89
	ethylene (C_2H_4)	8.4	303	0.89	2.91	1.69	0.84
			323	0.60	2.36	0.90	0.89
S1	ethane (C_2H_6)	5.8	303	0.22	2.18	0.26	0.88
			323	0.16	1.61	0.15	0.95
	ethylene (C_2H_4)	6.2	303	0.32	2.34	0.53	0.89
			323	0.22	1.96	0.31	0.88
S2	ethane (C_2H_6)	4.7	303	0.17	2.07	0.34	0.88
			323	0.12	1.44	0.29	0.91
	ethylene (C_2H_4)	4.6	303	0.25	0.86	0.36	1.06
			323	0.18	1.96	0.19	1.17
MCM-41	ethane (C_2H_6)	4.2	303	0.27	2.84	0.22	0.93
			323	0.18	2.57	0.08	0.92
	ethylene (C_2H_4)	5.0	303	0.48	2.32	0.60	0.92
			323	0.34	2.47	0.34	0.92

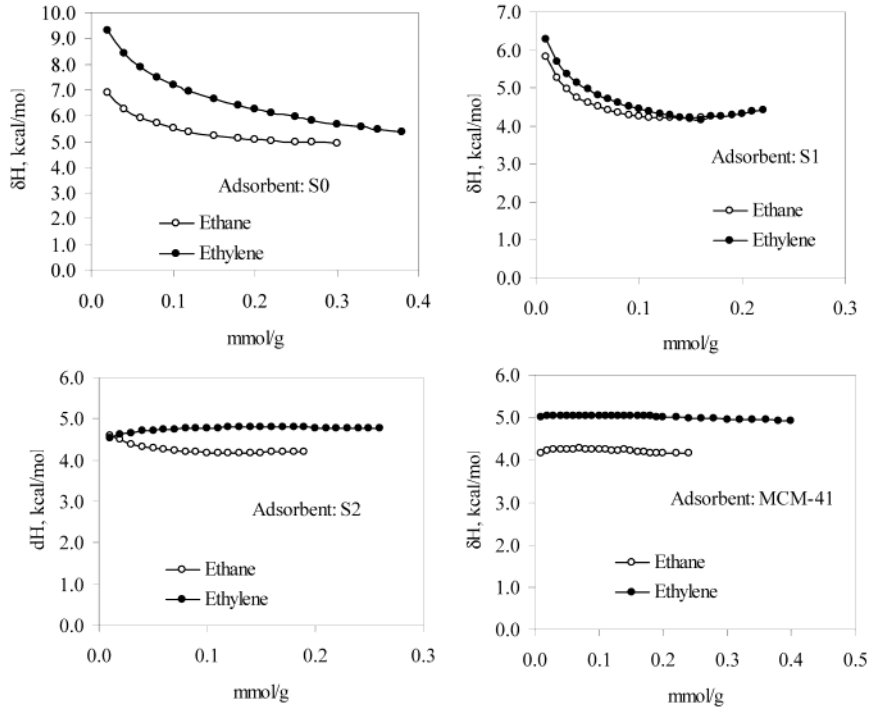

Figure 5. Dependence of isosteric heats of adsorption for ethane and ethylene on various adsorbent samples with coverage.

cant on S1 and was not seen on S2 and MCM-41 samples. Such a trend has also indicated the absence of specific adsorption sites on S2 and MCM-41 samples, thereby revealing the surface homogeneity of these adsorbents for ethylene molecules.

Role of Framework Porosity in Olefin Uptake. Recently reported structural elucidation studies on SBA-15 indicated the existence of micropores within the pore walls of its mesopores.[28] The origin of such micropores is ascribed to the hydrophilic nature of poly(ethylene oxide) (PEO) blocks of the template which causes them to occlude deeply within the silica walls. Upon calcination of these deeply occluded parts of the template, microporosity is generated in the framework.[28] On the other hand, such framework microporosity is completely absent for MCM-41-type frameworks. Furthermore, although specific sites for the adsorption of unsaturated molecules have been recently found to reside in these micropores, the role of the surface of SBA-15 in olefin uptake was not established.[20]

Recently, the control over such framework porosity was achieved in the presence of sodium chloride under microwave-hydrothermal conditions.[22] Furthermore, such approach also led to a decrease in mesopore size of SBA-15 framework. The control over framework porosity was reported to be achieved due to the rapid dehydration of PEO-blocks under the influence of microwaves and creation of rapid hydrophobic environment around the PEO−PPO−PEO micelles in the presence of sodium chloride, owing to its self-hydration behavior. This in turn resulted in the formation of micelles with a low hydrodynamic volume, thereby reducing the penetration of the PEO blocks inside the walls of the SBA-15 embryo, which is believed to lead to the formation of a mesoporous framework with low degree of framework microporosity and lower mesopore size as compared to those obtained under conventional hydrothermal approach.

As the adsorbents employed in the present investigation have varying degrees of framework microporosity,

the obtained trends provide us an ideal platform to understand and establish the influence of adsorption sites during olefin uptake on SBA-15-type frameworks. Therefore, an attempt has been made to correlate the uptake and heats of adsorption trends observed on various adsorbents in terms of their textural characteristics.

On the basis of the textural parameters, sample S0 is found to have the highest degree of framework microporosity followed by S1 and S2 and MCM-41. Therefore, the number of specific adsorption sites for olefin uptake can be visualized to increase in the order of S2 ~ MCM-41 < S1 < S0 on various adsorbents. This is what has been observed in the present study. The sample S0 displayed the highest uptake and affinity for olefins and the drop in such affinity and uptake on S1 and S2 samples reinforced the role of framework microporosity. Further, a good agreement between the heats of adsorption trends observed for samples S2 and MCM-41 clearly demonstrated the importance of framework microporosity in olefin uptake on SBA-15-like mesoporous frameworks.

Conclusion

The present study demonstrates the ability of mesoporous silica, SBA-15, for reversible uptake of light hydrocarbons and its selectivity for light alkenes. The adsorption selectivity is strongly influenced by framework porosity, and tailoring the framework porosity could result in control over adsorption selectivity. Thus the potential of SBA-15 as a suitable adsorbent for light hydrocarbon separation can be exploited by tailoring its textural characteristics.

Acknowledgment. B.L.N. and S.K. gratefully acknowledge the support of this work by the NSF MRSEC program under grant numbe DMR-0080019. N.V.C., P.K., V.R.P., and T.B. are thankful to the management of Indian Petrochemicals Corporation Limited (IPCL), Vadodara, India, for supporting this work. The authors are also thankful to S. P. Patel, IPCL, India, for his assistance during adsorption measurements.

CM020889D